Chapter 6

Discovery of Triazole Bridged Aryl Adamantane Analogs

6.1 Experimental Work

6.1.1 Rationale of drug design

The design strategy of multitarget-directed triazole bridged cycloaryl analogs is depicted in Figure 6.1. The amyloid hypothesis suggested that accumulation of Aβ in the brain is the primary influence driving AD pathogenesis. Aβ oligomerization starts within the cells rather than in the extracellular space [Walsh et al. 2000]. Aβ was shown to be produced in high amounts in synaptic terminals of the dentate gyrus of brain and deposited in extracellular plaques [Lazarov et al. 2002]. The cognitive function ultimately depends on synaptic plasticity, where long term potentiation (LTP) is associated with synapse growth and long term depression (LTD) is associated with synaptic loss. Aβ is associated with the inhibition of LTP[Walsh et al. 2002] and the promotion of LTD [Hunter et al. 2018, Li et al. 2009b]. Furthermore, concurrent exposure to Aβ and NMDAR synergistically increased [Ca^{2+}] levels, an effect mediated by GluN2B containing NMDARs [Ferreira et al. 2012]. All these theories evidently demonstrate that glutamate receptors are dysregulated by Aβ oligomers and subsequently in the disruption of glutamatergic synaptic transmission, which parallels early cognitive deficits. By compiling the ChE, Aβ and NMDR hypotheses, a novel strategy so-called MTDLs have been developed as a new hope for AD. In principle, combination of potent and distinct pharmacophoric groups to confer multiple activities and development of a novel hybrid analogs. A critical point in the design of MTDLs is the selection of targets and hence, of pharmacophores to be used.

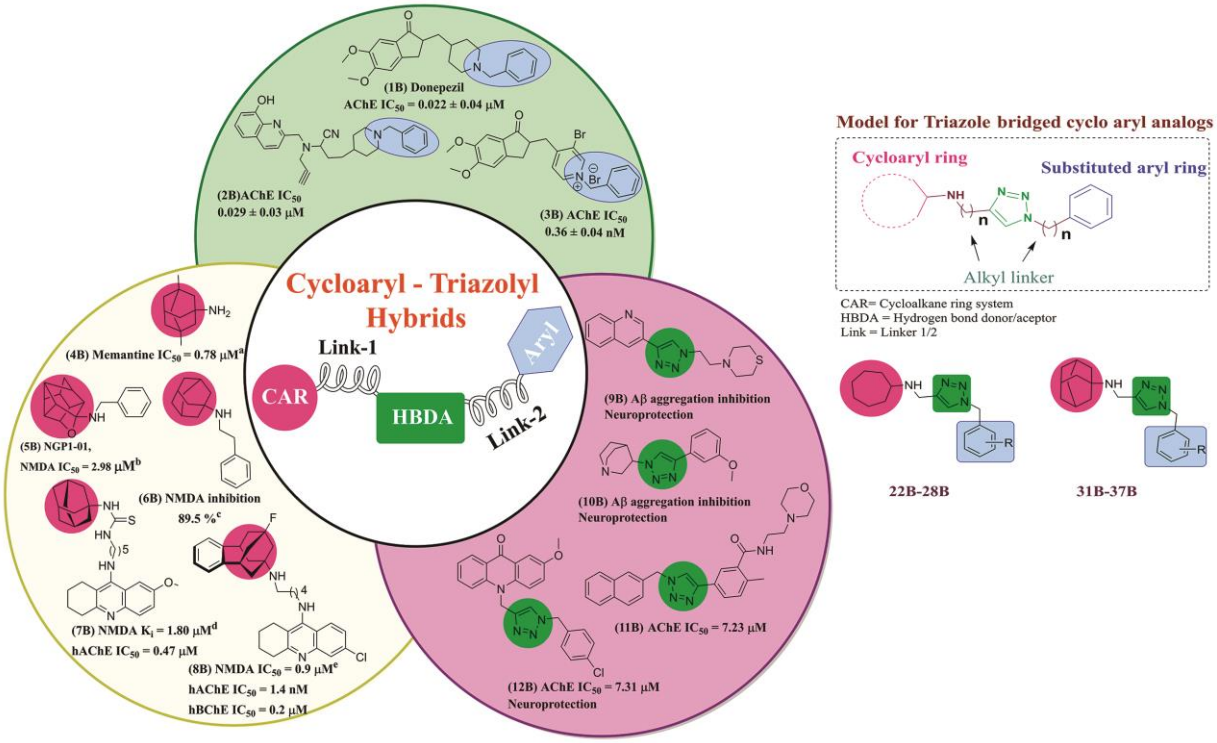

Figure 6.1. Drug design paradigm of multitarget-directed ligand Strategy for AD. [a]Two-electrode voltage clamp electrophysiology on GluN1-1a/GluN2B expressing oocytes. [b]NGP1-01-NMDA-mediated Ca^{2+} influx in synaptoneurosomes. [c]NMDA/glycine induced calcium influx (at 100 µM) and KCl induced calcium influx inhibition (at 100 µM). [d]Whole-cell voltage -clamp electrophysiology on GluN1 /GluN2B using HEK293 cells. [e]Intracellular calcium evoked by NMDA (100 µM, in the presence of 10 µM glycine) in cultured rat cerebellar granule neurons (CGN) loaded with Fura-2.

Here, we constructed a novel synthetic model by amalgamating the cycloary ring system and aromatic ring system bridged with a hydrogenbond donar/acceptor. For the initial screening, the cycloheptane and adamantine rings were chosen for cycloaryl ring system. Researchers developed a series of 7-methoxytacrine-adamantane (**7B**) [Gazova et al. 2017] and benzohomoadamantane chlorotacrine (**8B**)[Pérez-Areales et al. 2019] hybrids as potent multi target anti-alzheimer agents. Triazole containing analogs (**9B**, **10B**, **11B** and **12B**) [Jones et al. 2016, Li et al. 2016, Mohammadi-Khanaposhtani et al. 2015, Ouach et al. 2016] evidently showed Aβ aggregation inhibition and

neuroprotective properties. Triazole ring system was incorporated as hydrogenbond donar/acceptor system. On the other end of triazole ring, substituted benzyl ring system was created to retain the ChE inhibition activity. The interlinking of the three distinct pharmacophores was expected to enhance the therapeutic effect of the anti-AD agents.

6.1.2 Drug-likeness, BBB permeability and toxicity filtration

In-silico prediction of Drug-likliness, BBB permeability and toxicity of selected compounds was performed by using PreADMET web-based server (https://preadmet.bmdrc.kr/).

6.1.3 Synthesis and characterization

6.1.3.1 Scheme 1. Synthesis of compounds 22B-28B and 31B-37B[a].

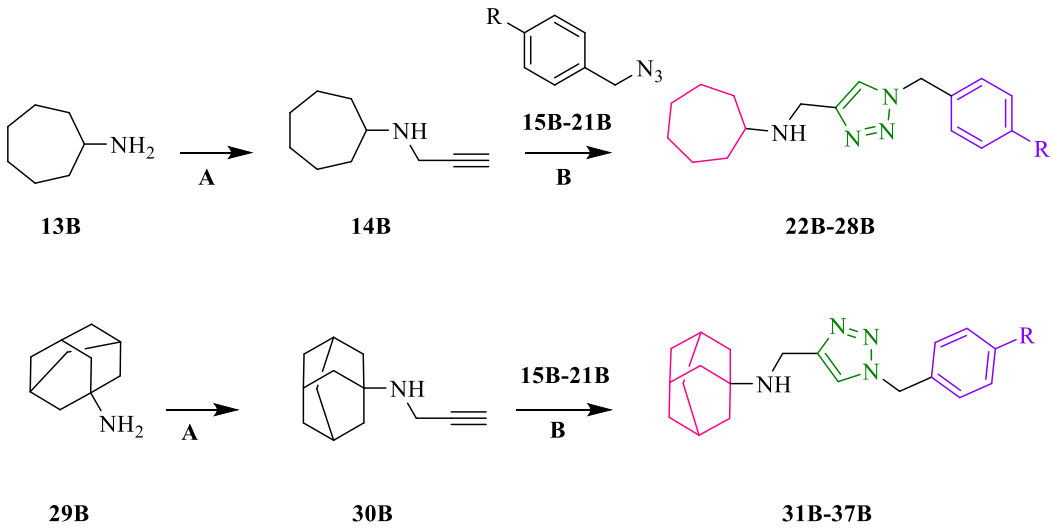

15B,22B,31B; R = H
16B,23B,32B; R = Bromo
17B,24B,33B; R = Chloro
18B,25B,34B; R = Fluoro

19B,26B,35B; R = Methyl
20B,27B,36B; R = Isopropyl
21B,28B,37B; R = Nitro

[a]Reagents and conditions: (A) Amine (**13B**/**29B**) 1.0 eq, Propargyl bromide 1.0 eq, Potassium carbonate 2.0 eq, DMF, rt, 6 h; (B) Compound (**14B**/**30B**) 1.0 eq, Substituted aryl azide (**15B-21B;** crude product) 1.2 eq, Diisopropylethylamine 1.0 eq, Copper(I) iodide (catalytic amount), DCM, rt, 12-16 h.

6.1.3.2 General procedure for the synthesis of 14B and 30B

A mixture of amine (**13B**/**29B**) (1.0 eq) and potassium carbonate (2.0 eq) in DMF (5 ml) was taken in a 50-mL round bottomed (R.B) flask with a magnetic stir bar, and then stirred thoroughly for 5 min at 0-5 °C. To it was added propargyl bromide (1.0 eq), and the reaction mixture was stirred at room temperature for 6 h. After completion of the reaction (monitored by TLC), mixture was subsequently partitioned between ethyl acetate (20 mL) and water (10 mL). The aqueous phase was extracted with ethyl acetate (2 × 5 mL). The combined organic extracts were washed with brine solution, dried over anhydrous sodium sulfate, filtered, and evaporated under reduced pressure. The obtained residue was purified by column chromatography on silica gel (60–120 mesh) to afford the desired compounds (**14B/ 30B)**.

N-(prop-2-yn-1-yl)cycloheptanamine **(14B)**: Brown oil, B.P.- 91-92 ℃, yield – 89%, ^{1}H NMR (500 MHz, $CDCl_3$) δ 3.42 (d, *J* = 2.5Hz, 2H, CH_2), 2.89 - 2.84 (Spt, 1H, cycloheptanamine C_1), 2.19 - 2.18 (t, 1H, acetylene CH), 1.82 - 1.39 (m, 12H, cycloheptanamine C_2 – C_7). ^{13}C NMR (125 MHz, $CDCl_3$) δ 82.51 (acetylene C_1), 70.91 (acetylene C_2), 57.02 (cycloheptanamine C_1), 35.65 (CH_2), 34.42 (cycloheptanamine C_2, C_7), 28.39 (cycloheptanamine C_4, C_5), 24.16 (cycloheptanamine C_3, C_6). MS (EI+):*m/z* calculated for $C_{10}H_{17}N$: 151.25, found – 152.61 (M+1).

N-(prop-2-yn-1-yl)adamantan-1-amine **(30B)**: Brown oil, B.P.- 102-103 ℃, yield – 85%, ^{1}H NMR (500 MHz, $CDCl_3$) δ 3.43 (d, *J* = 2.5Hz, 2H, CH_2), 2.20 (t, *J* = 2.5Hz, 1H, acetylene CH), 2.09 (s, 3H, adamantane C_3, C_5, C_7), 1.70 - 1.60 (m, 12H, adamantane C_2, C_4, C_6, C_8, C_9, C_{10}), 1.44 (bs, 1H, NH). ^{13}C NMR (125 MHz, $CDCl_3$) δ 83.93 (acetylene C_1), 70.56 (acetylene C_2), 50.96 (adamantane C_1), 42.59 (adamantane

C_2, C_8, C_{10}), 36.61 (adamantane C_4, C_6, C_9), 30.10 (CH_2), 29.53 (adamantane C_3, C_5, C_7). MS (EI+):*m/z* calculated for $C_{13}H_{19}N$: 189.3, found – 190.24 (M+1).

6.1.3.3 General procedure for the synthesis of 15B-21B

Compounds **15B-21B** were synthesized according to a previously described method and were used directly for the next step without further purification [Srivastava et al. 2015].

6.1.3.4 General procedure for the synthesis of 22B-28B; 31B-37B

To a stirring solution of compound **14B/30B** (1.0 equivalent) and aryl azide (**15B-21B**; 1.2 eq) in anhydrous dichloromethane (4 mL), CuI (0.5 mmol) and diisopropylethylamine (1.0 equiv) were added and stirring was continued at room temperature for 12-16 h under nitrogen atmosphere. After completion of reaction (monitored by TLC), the reaction mixture was concentrated *in vacuo* to obtain a crude residue, which was purified by column chromatography over silica gel (60-120 mesh) and ethyl acetate/*n*-hexanea as eluants, to afford desired triazole derivatives (**22B-28B; 31B-37B**).

*N-((1-benzyl-1H-1,2,3-triazol-4-yl)methyl)cycloheptanamine (***22B***)*: White solid, M.P.-124-125 °C, yield – 83%, ^{1}H NMR (500 MHz, $CDCl_3$) δ 7.41 (s, 1H, triazole C_5), 7.39 - 7.37 (m, 3H, benzyl C_3, C_4, C_5), 7.29 (s, 1H, benzyl C_2), 7.27 (s, 1H, benzyl C_6), 5.51 (s, 2H, benzyl CH_2), 3.90 (s, 2H, methyl CH_2), 2.74 - 2.70 (spt, 1H, cycloheptanamine C_1), 2.31 (bs, 1H, NH), 1.90 - 1.27 (m, 12H, cycloheptanamine C_2 – C_7). ^{13}C NMR (125 MHz, $CDCl_3$) δ 147.04 (benzyl C_1), 134.69 (triazole C_4), 129.09 (benzyl C_3, C_5), 128.71 (benzyl C_4), 128.12 (benzyl C_2, C_6), 121.63 (triazole C_5), 58.62 (benzyl CH_2), 54.13 (cycloheptanamine C_1), 42.32 (methyl CH_2), 34.46 (cycloheptanamine C_2), 29.70 (cycloheptanamine C_7), 28.28 (cycloheptanamine C_4, C_5), 24.30 (cycloheptanamine C_3, C_6). MS (EI+):*m/z* calculated for $C_{17}H_{24}N_4$: 284.41, found – 285.37 (M+1).

*N-((1-(4-bromobenzyl)-1H-1,2,3-triazol-4-yl)methyl)cycloheptanamine (***23B***)*: White solid, M.P.- 111-112 ℃, yield – 87%, ^{1}H NMR (500 MHz, $CDCl_3$) δ 7.51 (d, *J* = 8.5Hz, 2H, 4-bromobenzyl C_3, C_5), 7.46 (s, 1H, triazole C_5), 7.15 (d, *J* = 8.5Hz, 2H, 4-bromobenzyl C_2, C_6), 5.47 (s, 2H, benzyl CH_2), 3.90 (s, 2H, methyl CH_2), 2.72 (bs, 1H, cycloheptanamine C_1), 2.38 (bs, 1H, NH), 1.87 - 1.41 (m, 12H, cycloheptanamine C_2 – C_7). ^{13}C NMR (125 MHz, $CDCl_3$) δ 133.69 (4-bromobenzyl C_1), 132.25 (4-bromobenzyl C_3, C_5, triazole C_4), 129.71 (4-bromobenzyl C_2, C_6), 122.89 (4-bromobenzyl C_4), 121.77 (triazole C_5), 58.61 (benzyl CH_2), 53.42 (cycloheptanamine C_1), 42.24 (methyl CH_2), 34.40 (cycloheptanamine C_2), 29.70 (cycloheptanamine C_7), 28.26 (cycloheptanamine C_4, C_5), 24.28 (cycloheptanamine C_3, C_6). MS (EI+):*m/z* calculated for $C_{17}H_{23}BrN_4$: 363.3, found – 364.21 (M+1), 365.47 (M+2).

*N-((1-(4-chlorobenzyl)-1H-1,2,3-triazol-4-yl)methyl)cycloheptanamine (***24B***)* : Off white solid, M.P.- 132-133 ℃, yield – 82%, ^{1}H NMR (500 MHz, $CDCl_3$) δ 7.38 (d, *J* = 8.5Hz, 2H, 4-chlorobenzyl C_3, C_5), 7.26 (s, 1H, triazole C_5), 7.20 (d, *J* = 8.5Hz, 2H, 4-chlorobenzyl C_2, C_6), 5.58 (s, 2H, benzyl CH_2), 3.83 (s, 2H, methyl CH_2), 2.19 (bs, 1H, cycloheptanamine C_1), 2.02 (bs, 1H, NH), 1.70 - 1.39 (m, 12H, cycloheptanamine C_2 – C_7). ^{13}C NMR (125 MHz, $CDCl_3$) δ 133.56 (4-chlorobenzyl C_1), 131.52 (4-chlorobenzyl C_4), 129.71 (triazole C_4), 129.24 (4-chlorobenzyl C_3, C_5), 126.26 (4-chlorobenzyl C_2, C_6), 121.41 (triazole C_5), 58.72 (benzyl CH_2), 53.31 (cycloheptanamine C_1), 41.75 (methyl CH_2), 34.27 (cycloheptanamine C_2), 29.21 (cycloheptanamine C_7), 28.35 (cycloheptanamine C_4, C_5), 24.61 (cycloheptanamine C_3, C_6). MS (EI+):*m/z* calculated for $C_{17}H_{23}ClN_4$: 318.85, found – 319-54 (M+1), 320.47(M+2).

*N-((1-(4-fluorobenzyl)-1H-1,2,3-triazol-4-yl)methyl)cycloheptanamine (***25B***)* : Yellow solid, M.P.- 115-116 ℃, yield – 85%, ^{1}H NMR (500 MHz, $CDCl_3$) δ 7.54 (d, *J* = 8.5Hz,

2H, 4-fluorobenzyl C_3, C_5), 7.49 (s, 1H, triazole C_5), 7.19 (d, *J* = 8.5Hz, 2H, 4-fluorobenzyl C_2, C_6), 5.45 (s, 2H, benzyl CH_2), 3.92 (s, 2H, methyl CH_2), 2.69 (bs, 1H, cycloheptanamine C_1), 2.32 (bs, 1H, NH), 1.81 - 1.42 (m, 12H, cycloheptanamine C_2 – C_7). ^{13}C NMR (125 MHz, $CDCl_3$) δ 158.4 (4-fluorobenzyl C_4) 132.48 (4-fluorobenzyl C_1), 130.25 (triazole C_4), 129.71 (4-fluorobenzyl C_2, C_6), 121.76 (triazole C_5), 114.75 (4-fluorobenzyl C_3, C_5,), 58.24 (benzyl CH_2), 53.37 (cycloheptanamine C_1), 42.28 (methyl CH_2), 34.35 (cycloheptanamine C_2), 29.61 (cycloheptanamine C_7), 28.32 (cycloheptanamine C_4, C_5), 24.26 (cycloheptanamine C_3, C_6). MS (EI+):*m/z* calculated for $C_{17}H_{23}FN_4$: 302.40, found – 303.25 (M+1).

*N-((1-(4-methylbenzyl)-1H-1,2,3-triazol-4-yl)methyl)cycloheptanamine (***26B***)* : Off white solid, M.P.- 134-135 ℃, yield – 88%, ^{1}H NMR (500 MHz, $CDCl_3$) δ 7.41 (s, 1H, triazole C_5), 7.17 (4-methylbenzyl C_2, C_3, C_5, C_6), 5.46 (s, 2H, benzyl CH_2), 3.88 (s, 2H, methyl CH_2), 2.71 (bs, 1H, cycloheptanamine C_1), 2.39 (bs, 1H, NH), 2.35 (s, 3H, CH_3), 1.89 - 1.26 (m, 12H, cycloheptanamine C_2 – C_7). ^{13}C NMR (125 MHz, $CDCl_3$) δ 146.80 (4-methylbenzyl C_4), 138.63 (4-methylbenzyl C_1), 131.65 (triazole C_4), 129.73 (4-methylbenzyl C_3, C_5), 128.17 (4-methylbenzyl C_2, C_6), 121.63 (triazole C_5), 58.56 (benzyl CH_2), 53.93 (cycloheptanamine C_1), 42.27 (methyl CH_2), 34.41 (cycloheptanamine C_2), 29.70 (cycloheptanamine C_7), 28.27 (cycloheptanamine C_4, C_5), 24.28 (cycloheptanamine C_3, C_6), 21.15 (4-methylbenzyl CH_3). MS (EI+):*m/z* calculated for $C_{18}H_{26}N_4$: 298.43, found – 299.31 (M+1).

*N-((1-(4-isopropylbenzyl)-1H-1,2,3-triazol-4-yl)methyl)cycloheptanamine (***27B***)* : Off white solid, M.P.- 126-127 ℃, yield – 86%, ^{1}H NMR (500 MHz, $CDCl_3$) δ 7.31 (bs, 2H, isopropylbenzyl C_3, C_5), 7.26 (s, 1H, triazole C_5), 7.11 (bs, 2H, isopropylbenzyl C_2, C_6), 5.57 (s, 2H, benzyl CH_2), 4.32 (s, 2H, methyl CH_2), 3.00 (bs, 1H, NH), 2.93 (m,

1H, cycloheptanamine C_1), 2.19 (m, 1H, isopropyl CH), 1.70 – 1.41 (m, 12H, cycloheptanamine C_2 – C_7), 1.27 – 1.26 (d, *J* = 5.5Hz, 6H, isopropyl CH_3*2). ^{13}C NMR (125 MHz, $CDCl_3$) δ 146.2 (isopropylbenzyl C_4), 133.45 (isopropylbenzyl C_1), 130.52 (triazole C_4), 127.31 (isopropylbenzyl C_2, C_6), 126.75 (isopropylbenzyl C_3, C_5), 121.87 (triazole C_5), 57.72 (benzyl CH_2), 55.26 (cycloheptanamine C_1), 44.74 (methyl CH_2), 33.41 (isopropyl CH), 34.24 (cycloheptanamine C_2, C_7), 28.37 (cycloheptanamine C_4, C_5), 24.17 (cycloheptanamine C_3, C_6). MS (EI+):*m/z* calculated for $C_{20}H_{30}N_4$: 326.49, found – 327.61 (M+1).

*N-((1-(4-nitrobenzyl)-1H-1,2,3-triazol-4-yl)methyl)cycloheptanamine (***28B***)* : Pale brown solid, M.P.- 142-143 °C, yield – 88%, ^{1}H NMR (500 MHz, $CDCl_3$) δ 8.24 - 8.22 (dt, *J* = 9Hz, 2H, 4-nitrobenzyl C_3, C_5), 7.51 (s, 1H, triazole C_5), 7.42 (d, 2H, 4-nitrobenzyl C_2, C_6), 5.63 (s, 2H, benzyl CH_2), 3.92 (s, 2H, methyl CH_2), 2.74 - 2.70 (m, 1H, cycloheptanamine C_1), 2.01 (bs, 1H, NH), 1.90 - 1.40 (m, 12H, cycloheptanamine C_2 – C_7). ^{13}C NMR (125 MHz, $CDCl_3$) δ 148.06 (4-nitrobenzyl C_4), 147.83 (4-nitrobenzyl C_1), 141.77 (triazole C_4), 128.60 (4-nitrobenzyl C_2, C_6), 124.28 (4-nitrobenzyl C_3, C_5), 121.91 (triazole C_5), 58.69 (benzyl CH_2), 53.06 (cycloheptanamine C_1), 42.34 (methyl CH_2), 34.55 (cycloheptanamine C_2, C_7), 28.28 (cycloheptanamine C_4, C_5), 24.27 (cycloheptanamine C_3, C_6). MS (EI+):*m/z* calculated for $C_{17}H_{23}N_5O_2$: 329.40, found – 330.24 (M+1).

*N-((1-benzyl-1H-1,2,3-triazol-4-yl)methyl)adamantan-1-amine (***31B***)* : Off white solid, M.P.- 115-116 °C, yield – 85%, ^{1}H NMR (500 MHz, $CDCl_3$) δ 7.51 (s, 1H, triazole C_5), 7.39 - 7.36 (m, 4H, benzyl C_2, C_3, C_5, C_6), 7.27 (m, 1H, benzyl C_4), 5.50 (s, 2H, benzyl CH_2), 3.96 (s, 2H, methyl CH_2), 3.19 (bs, 1H, NH), 2.11 - 1.27 (m, 15H, adamantane C_2, C_3, C_4, C_5, C_6, C_7, C_8, C_9, C_{10}). ^{13}C NMR (125 MHz, $CDCl_3$) δ 146.72 (benzyl C_1),

134.66 (triazole C_4), 129.07 (benzyl C_3, C_5), 128.70 (benzyl C_4), 128.15 (benzyl C_2, C_6), 122.11 (triazole C_5), 54.15 (benzyl CH_2), 52.02 (adamantane C_1), 41.90 (adamantane C_2, C_8, C_{10}), 36.49 (adamantane C_4, C_6, C_9), 35.94 (CH_2), 29.48 (adamantane C_3, C_5, C_7). MS (EI+):*m/z* calculated for $C_{20}H_{26}N_4$: 322.46, found – 323.64 (M+1).

*N-((1-(4-bromobenzyl)-1H-1,2,3-triazol-4-yl)methyl)adamantan-1-amine (***32B***)* : White solid, M.P.- 124-125 ℃, yield – 85%, ^{1}H NMR (500 MHz, $CDCl_3$) δ 7.51 - 7.49 (m, 3H, triazole C_5, 4-bromobenzyl C_3, C_5), 7.16 (d, *J* = 8.5Hz, 2H, 4-bromobenzyl C_2, C_6), 5.45 (s, 2H, benzyl CH_2), 3.91 (s, 2H, methyl CH_2), 2.24 (bs, 1H, NH), 2.10 (s, 3H, adamantane C_3, C_5, C_7) 1.71 - 1.61 (m, 12H, adamantane C_2, C_4, C_6, C_8, C_9, C_{10}). ^{13}C NMR (125 MHz, $CDCl_3$) δ 147.90 (4-bromobenzyl C_1), 133.73 (triazole C_4), 132.23 (4-bromobenzyl C_3, C_5), 129.75 (4-bromobenzyl C_2, C_6), 122.85 (4-bromobenzyl C_4), 121.80 (triazole C_5), 53.42 (benzyl CH_2), 51.41 (adamantane C_1), 42.34 (adamantane C_2, C_8, C_{10}), 36.59 (adamantane C_4, C_6, C_9), 36.20 (CH_2), 29.54 (adamantane C_3, C_5, C_7). MS (EI+):*m/z* calculated for $C_{20}H_{25}BrN_4$: 401.35, found – 402.55 (M+1), 403.62 (M+2).

*N-((1-(4-chlorobenzyl)-1H-1,2,3-triazol-4-yl)methyl)adamantan-1-amine (***33B***)* : White solid, M.P.- 125-126 ℃, yield – 93%, ^{1}H NMR (500 MHz, $CDCl_3$) δ 7.57 (s, 1H, triazole C_5), 7.35 (d, *J* = 8Hz, 2H, 4-chlorobenzyl C_3, C_5), 7.22 (d, *J* = 8Hz, 2H, 4-chlorobenzyl C_2, C_6), 5.48 (s, 2H, benzyl CH_2), 3.90 (s, 2H, methyl CH_2), 2.18 - 2.17 (m, 4H, adamantane C_3, C_5, C_7, NH), 1.72 - 1.63 (m, 12H, adamantane C_2, C_4, C_6, C_8, C_9, C_{10}). ^{13}C NMR (125 MHz, $CDCl_3$) δ 134.78 (4-chlorobenzyl C_1), 133.11 (triazole C_4), 131.85 (4-chlorobenzyl C_4), 129.51 (4-chlorobenzyl C_3, C_5), 129.25 (4-chlorobenzyl C_2, C_6), 121.82 (triazole C_5), 53.71 (benzyl CH_2), 52.34 (adamantane C_1), 42.51 (adamantane C_2, C_8, C_{10}), 36.54 (adamantane C_4, C_6, C_9), 36.53 (CH_2), 29.69

(adamantane C_3, C_5, C_7). MS (EI+):*m/z* calculated for $C_{20}H_{25}ClN_4$: 356.9, found – 357.87 (M+1), 358.34 (M+2).

*N-((1-(4-fluorobenzyl)-1H-1,2,3-triazol-4-yl)methyl)adamantan-1-amine (***34B***)* : White solid, M.P.- 134-135 °C, yield – 84%, ^{1}H NMR (500 MHz, $CDCl_3$) δ 7.62 (s, 1H, triazole C_5), 7.37 (d, *J* = 8Hz, 2H, 4-fluorobenzyl C_3, C_5), 7.23 (bs, 2H, 4-fluorobenzyl C_2, C_6), 5.37 (s, 2H, benzyl CH_2), 3.78 (s, 2H, methyl CH_2), 2.17 - 2.16 (m, 4H, adamantane C_3, C_5, C_7, NH), 1.76 - 1.65 (m, 12H, adamantane C_2, C_4, C_6, C_8, C_9, C_{10}). ^{13}C NMR (125 MHz, $CDCl_3$) δ 158.6 (4-fluorobenzyl C_4), 132.41 (4-fluorobenzyl C_1), 130.25 (triazole C_4), 128.41 (4-fluorobenzyl C_2, C_6), 122.64 (triazole C_5), 115.82 (4-fluorobenzyl C_3, C_5,), 55.65 (benzyl CH_2), 52.27 (adamantane C_1), 42.27 (adamantane C_2, C_8, C_{10}), 36.51 (adamantane C_4, C_6, C_9), 36.52 (CH_2), 29.67 (adamantane C_3, C_5, C_7). MS (EI+):*m/z* calculated for $C_{20}H_{25}FN_4$: 340.45, found – 341.28 (M+1).

*N-((1-(4-methylbenzyl)-1H-1,2,3-triazol-4-yl)methyl)adamantan-1-amine (***35B***)* : White solid, M.P.- 131-132 °C, yield – 86%, ^{1}H NMR (500 MHz, $CDCl_3$) δ 7.62 (s, 1H, triazole C_5), 7.32 (d, *J* = 8Hz, 2H, 4-methylbenzyl C_3, C_5), 7.21 (d, *J* = 8Hz, 2H, 4-methylbenzyl C_2, C_6), 5.41 (s, 2H, benzyl CH_2), 3.78 (s, 2H, methyl CH_2), 2.32 (s, 3H, CH_3), 2.18 - 2.17 (m, 4H, adamantane C_3, C_5, C_7, NH), 1.71 - 1.64 (m, 12H, adamantane C_2, C_4, C_6, C_8, C_9, C_{10}). ^{13}C NMR (125 MHz, $CDCl_3$) δ 135.24 (4-methylbenzyl C_4), 133.41 (4-methylbenzyl C_1), 130.11 (triazole C_4), 129.42 (4-methylbenzyl C_3, C_5), 127.24 (4-methylbenzyl C_2, C_6), 121.86 (triazole C_5), 55.63 (benzyl CH_2), 52.57 (adamantane C_1), 42.52 (adamantane C_2, C_8, C_{10}), 36.54 (adamantane C_4, C_6, C_9), 36.52 (CH_2), 29.69 (adamantane C_3, C_5, C_7), 21.52 (CH_3). MS (EI+):*m/z* calculated for $C_{21}H_{28}N_4$: 336.48, found – 337.34 (M+1).

*N-((1-(4-isopropylbenzyl)-1H-1,2,3-triazol-4-yl)methyl)adamantan-1-amine (***36B***)* : White solid, M.P.- 115-116 ℃, yield – 89%, ^{1}H NMR (500 MHz, $CDCl_3$) δ 7.22 (bs, 3H, triazole C_5, 4-isopropylbenzyl C_3, C_5), 7.15 (bs, 2H, 4-isopropylbenzyl C_2, C_6), 5.51 (s, 2H, benzyl CH_2), 4.33 (s, 3H, methyl CH_2, NH), 2.95 – 2.88 (spt, 1H, isopropyl CH), 2.09 (s, 3H, adamantane C_3, C_5, C_7) 1.77 - 1.44 (m, 12H, adamantane C_2, C_4, C_6, C_8, C_9, C_{10}), 1.23 – 1.22 (d, *J* = 5Hz, 6H, isopropyl CH_3*2). ^{13}C NMR (125 MHz, $CDCl_3$) δ 145.27 (4-isopropylbenzyl C_4), 133.57 (4-isopropylbenzyl C_1), 130.73 (triazole C_4), 127.23 (4-isopropylbenzyl C_3, C_5), 126.75 (4-isopropylbenzyl C_2, C_6), 122.41 (triazole C_5), 53.41 (benzyl CH_2), 51.53 (adamantane C_1), 42.21 (adamantane C_2, C_8, C_{10}), 36.52 (adamantane C_4, C_6, C_9), 36.34 (CH_2), 33.24 (isopropyl CH), 29.35 (adamantane C_3, C_5, C_7), 23.47 (isopropyl CH_3*2). MS (EI+):*m/z* calculated for $C_{23}H_{32}N_4$: 364.54, found – 365.51 (M+1).

*N-((1-(4-nitrobenzyl)-1H-1,2,3-triazol-4-yl)methyl)adamantan-1-amine (***37B***)* : White solid, M.P.- 137-138 ℃, yield – 92%, ^{1}H NMR (500 MHz, $CDCl_3$) δ 8.24 - 8.21 (dt, *J* =8.5, 2.5 Hz, 4-nitrobenzyl C_3, C_5), 7.55 (s, 1H, triazole C_5), 7.43 (d, *J* = 9Hz, 4-nitrobenzyl C_2, C_6), 5.63 (s, 2H, benzyl CH_2), 3.93 (s, 2H, methyl CH_2), 2.11 (bs, 3H, adamantane C_3, C_5, C_7,), 1.96 (bs, 1H, NH), 1.71 - 1.62 (m, 12H, adamantane C_2, C_4, C_6, C_8, C_9, C_{10}). ^{13}C NMR (125 MHz, $CDCl_3$) δ 148.05 (4-nitrobenzyl C_4), 141.78 (4-nitrobenzyl C_1), 128.65 (4-nitrobenzyl C_3, C_5), 124.26 (4-nitrobenzyl C_2, C_6, triazole C_4), 122.00 (triazole C_5), 53.08 (benzyl CH_2), 51.22 (adamantane C_1), 42.49 (adamantane C_2, C_8, C_{10}), 36.61 (adamantane C_4, C_6, C_9), 36.23 (CH_2), 29.56(adamantane C_3, C_5, C_7). MS (EI+):*m/z* calculated for $C_{20}H_{25}N_5O$: 367.45, found – 368.32 (M+1).

6.1.4 Biological evaluation

6.1.4.1 Evaluation of cholinesterase inhibitory activities (*ee*AChE and *eq*BuChE)

Chapter 5, section 5.1.4.1 contains the detailed procedure of assay. Briefly, six different working concentrations (0.001 μM, 0.01 μM, 0.1 μM, 1 μM, 10 μM, and 50 μM) of test compounds were used in the enzyme inhibition studies.

6.1.4.2 Evaluation of blood-brain barrier permeability: PAMPA assay

The details of assay protocol is mentioned in chapter 4, section 4.1.4.2. The concentration of drug in acceptor, donor and reference wells were determined by UV spectroscopy. Each sample was scanned to at least five different wavelengths and in three independent runs.

6.1.4.3 Propidium iodide (PI) displacement assay

The detailed assay protocol is included in chapter 4, section 4.1.4.3. Fluorescence intensity was measured after 10 min, at excitation and emission wavelength of 535 nm and 595 nm, respectively using microplate reader (HTX multi-mode reader, BioTek, USA).

6.1.4.4 Evaluation of NMDA receptor activity

6.1.4.4.1 Cloning and RNA synthesis

The investigation of NMDA receptors in *Xenopus laevis* oocytes included all cDNAs (GluN1-1a, GluN1-1b, GluN2A, GluN2B, GluN2C and GluN2D) that were previously cloned into the pSGEM vector. For oocyte injection, complementary RNA (cRNA) was generated from 1 μg of linearized template cDNA using the mMESSAGE mMACHINE™ T7 *in vitro* transcription kit (Thermo Fisher Scientific).

6.1.4.4.2 Electrophysiological studies in *Xenopus laevis* oocytes

The parts of the ovaries of *Xenopus laevis* (Nasco) were anesthetized with 3-aminobenzoic acid ethyl ester (1.5 g/l, Sigma), were surgically removed and subsequently digested for 1.5–2 h with collagenase type I (186 U/ml, 4 mg/ml, Worthington) in Ca^{2+}-free Barth's medium (88 mM NaCl, 1.1 mM KCl, 2.4 mM $NaHCO_3$, 0.8 mM $MgSO_4$, 15 mM Hepes-NaOH, pH 7.6) at 20 °C to remove the follicular cell layer and to separate the oocytes. After ceasing the collagenase digestion by rinsing the oocytes, several times, with Ca^{2+}-containing Barth's medium (88 mM NaCl, 1.1 mM KCl, 2.4 mM $NaHCO_3$, 0.3 mM $Ca(NO_3)_2$, 0.4 mM $CaCl_2$, 0.8 mM $MgSO_4$, 15 mM Hepes-NaOH, pH 7.6), oocytes of stages V and VI were selected and maintained at 17 °C in Ca^{2+}-containing Barth's medium supplemented with gentamicin (40 μg/mL), streptomycin (40 μg /ml) and penicillin (63 μg /ml). The expression of the desired diheteromeric receptors was achieved by injecting 0.5–2 fmol of each cRNA into the oocytes using a nanoliter injector (WPI).

Electrophysiological measurements were performed 1–5 days after cRNA injection, using the two-electrode voltage clamp technique at a holding potential of -70 mV with a Turbo Tec-10CX amplifier (npi electronic) controlled by Pulse software (HEKA). The currents were recorded with a 20-Hz low-pass filter and subsequently digitized with a sampling rate of 50 Hz. The recording electrodes were made by inserting a Ag/AgCl electrode into a pipette that was pulled from borosilicate glass (Science Products) with a vertical pipette puller (PIP 5, HEKA) and filled with 3 M KCl. The electrodes had resistances of 0.5–5 MΩ (voltage electrode) and 0.5–1.5 MΩ (current electrode), respectively. Recordings were performed in Ba^{2+}-containing Ringer's solution (BaR, 115 mM NaCl, 2.5 mM KCl, 1.8 mM $BaCl_2$, 10 mM Hepes-NaOH, pH 7.2). To record

the dose-inhibition curves, the receptors were first activated by the application of agonists at saturating concentrations (10 μM glycine and 100 μM L-glutamate) until an equilibrium response was reached. Further, the increasing concentrations of the test compound in concentrations of 0.01 μM – 1 mM were co-applied with the agonists for 20 s to the same oocyte. The resulting equilibrium currents in the presence of antagonist were divided by the current recorded in presence of agonists alone to calculate the inhibition. The reversibility was checked by applying the agonists again after application of the antagonists. The IC_{50} values were calculated by taking the average inhibition data, from at least three independent oocytes, to the Hill equation using Prism (Graph Pad). All the recordings were repeated at least one time.

6.1.4.5 Evaluation of $A\beta_{1-42}$ anti-aggregation properties

The detail of assay protocol is provided in chapter 5, section 5.1.4.4. Three concentrations (5 μM, 10 μM, and 20 μM) of test compounds were used in the enzyme inhibition studies. Fluorescence intensity was measured after incubation time, at excitation and emission wavelengths of 450 nm and 485 nm, respectively using microplate reader (HTX multi-mode reader, BioTek, USA).

6.1.4.6 Neuroprotection studies on SH-SY5Y cell lines

The details of the assay protocols is included in chapter 5, section 5.1.4.5. Four concentrations (0.1 μM, 1 μM, 10 μM, and 100 μM) of test compounds were used in the neuroprotection studies. The absorbance was measured at 570 nm, and the % cell viability was calculated. Each treatment was executed in triplicate and data are presented as percentage of the control.

6.2 Results and Discussion

6.2.1 Drug-likeliness, ADME and toxicity Prediction

Chemical absorption, distribution, metabolism, excretion, and toxicity (ADMET), play key roles in drug discovery and development. A high-quality drug candidate should not only have sufficient efficacy against the therapeutic target, but also should show appropriate ADMET properties at a therapeutic dose. A lot of *in silico* models are hence developed for prediction of chemical ADMET properties. The designed compounds were evaluated for their ADME and toxicity predictions by using preADMET server. The predicted properties included blood-brain barrier (BBB) permeability, buffer solubility, hERG inhibition, Caco-2 cell permeability, human intestinal absorption and carcinogenicity (Mouse). The properties were calculated and the results are summarized in Table 6.1.

6.2.2 Synthesis of triazole bridged cycloaryl analogs and their characterization

The synthetic strategy for target triazole bridged cycloaryl analogs **22B-28B** and **31B-37B** is depicted in section 6.1.3.1, scheme 1. Briefly, the reaction was started from the nucleophilic aliphatic substitution reaction of cycloheptylamine (**13B**) /adamantine (**29B**) amine with propargyl bromide. The obtained secondary amines (**14B**/**30B**) were utilized to synthesize triazole bridged cycloaryl analogs by Huisgen's 1,3-dipolar cycloaddition. The substituted aryl azide (**15B-21B**) was reacted with **14B**/**30B** in presence of catalytic amount of CuI and DIPEA as an organic base. The isolated compounds were characterized by NMR (^{1}H and ^{13}C) and Mass spectrometry. The identification of triazole C5' proton and two methylene (CH_2) peaks in ^{1}H and ^{13}C NMR helped for the preliminary characterization. The remaining aliphatic and aromatic

protons were also identified for respective compounds. The % purity of the final analogs were assessed with HPLC analysis (Shimadzu LC solutions).

6.2.3 *In-vitro* cholinesterase inhibition (*ee*AChE and *eq*BuChE)

The potency and selectivity of the newer analogs to AChE are always the driving force while developing promising AChEIs. Accurate binding dynamics towards AChE and balanced regulation of different AChE isoforms may enhance the therapeutic efficacies of AChEIs. Thus, precise regulation of AChE activation may help to optimize the therapeutic efficacies of AChEIs. All the synthesized triazole bridged cycloaryl analogs (**22B-28B** and **31B-37B**) were designed to investigate the inhibitory potentials against AChE and BuChE. DNZ was used as a positive reference standard. Cycloheptane containing triazole aryl analogs (**22B-28B**) exhibited moderate inhibitory potential against AChE and BuChE. The adamantine containing analogs (**31B-37B**) demonstrated better inhibitory profiles as compared to cycloheptane analogs. The *para*-bromo substituted derivative of adamantine analog (**32B**: AChE IC_{50} = 0.086 μM; BuChE IC_{50} = 2.54 μM) and *para*-chloro substituted derivative (**33B**: AChE IC_{50} = 0.135 μM; BuChE IC_{50} = 3.79 μM) turned out to be potent AChE inhibition. Whereas, *para*-nitro derivatives in both series (**28B**: AChE IC_{50} = 4.637 μM; BuChE IC_{50} = 19.21 μM and **37B**: AChE IC_{50} = 1.608 μM; BuChE IC_{50} = 19.21 μM) showed lower inhibition. The presence of adamantine ring in these hybrids (**31B-37B**) seems to be responsible for the better inhibitions against ChEs. Further, exploration of cycloaryl scaffold and subtitutions on phenyl ring would provide the greater insights in the drug development for AD.

6.2.4 *In-vitro* blood-brain barrier permeation assay

As a preliminary assessment of brain permeability, the novel triazole bridged cycloaryl analogs were subjected to parallel artificial membrane permeation assay-BBB (PAMPA-BBB), a well-established *in-vitro* model of passive trans cellular permeation [Di et al. 2003a]. The assay was validated by correlating the experimental and reported Pe values of 9 known drugs. The *Pe* values of compounds (**22B-28B & 31B-37B**) are listed in Table 6.2. All the triazole bridged cycloaryl analogs of the cycloheptane and adamantine ring, were predicted to be able to cross the BBB, which anticipated their ability to enter the brain and reach their different CNS targets. The compound **32B** (Pe = 8.75 ± 0.017 * 10^{-6} cm s^{-1}) and **33B** (Pe = 8.24 ± 0.034 * 10^{-6} cm s^{-1}) showed appreciable BBB permeability.

6.2.5 Propidium iodide displacement assay

To support our ChE hypothesis that designed analogs would bind efficiently with PAS-AChE, propidium iodide displacement assay was conducted for the selected MTDLs using the method described by Taylor et al [Taylor and Lappi 1975]. Propidium iodide is the known ligand, selectively binding to PAS-AChE and displaying increased fluorescence intensity up to 8- to 10- folds [Taylor et al. 1974]. The decreased fluorescence intensity can be estimated as the percentage propidium iodide displacement from PAS-AChE due to the presence of inhibitor at 10 μM and 50 μM concentrations. The results are shown in Table 6.3. The compounds **32B** (10 μM: 20.96%; 50 μM: 40.93%) and **33B** (10 μM: 19.96%; 50 μM: 34.10%) demonstrated remarkable propidium iodide displacement capability compared to DNZ (10 μM: 20.34%; 50 μM: 36.61%).

Table 6.1: ADME and toxicity prediction of the compounds.

Comp. No	BBB[a]	Buffer solubility (mg/L)[b]	hERG Inhibition[c]	Caco-2 cell permeability (nm/sec)[d]	Human intestinal absorption (HIA, %)	Carcinogenicity (Mouse)
22B	0.477	29.015	Medium risk	23.6436	95.614	Negative
23B	1.333	8.345	Medium risk	40.6438	96.299	Negative
24B	1.200	17.680	Medium risk	41.1017	95.990	Negative
25B	0.674	55.629	Medium risk	48.5271	95.618	Negative
26B	0.954	20.817	Medium risk	25.42	95.679	Negative
27B	2.380	6.703	Medium risk	27.4369	95.833	Negative
28B	0.020	5.851	Medium risk	18.6641	93.966	Negative
31B	0.364	34.573	Medium risk	28.2464	95.834	Negative
32B	1.071	9.689	Medium risk	30.1553	96.562	Negative
33B	0.957	20.799	Medium risk	30.2122	96.270	Negative
34B	0.521	65.819	Medium risk	36.9472	95.840	Negative
35B	0.743	24.667	Medium risk	30.8389	95.920	Negative
36B	1.975	7.865	Medium risk	33.6623	96.104	Negative
37B	0.026	6.859	Medium risk	20.335	96.052	Negative

[a]*In vivo* blood-brain barrier penetration (C.brain/C.blood). [b]Water solubility in buffer system (SK atomic types, mg/L). [c]Human ether –a-go-go related gene channel inhibition. [d] *In vitro* Caco2 cell permeability (Human colorectal carcinoma).

Table 6.2 : Structures, cholinesterase (*ee*AChE and *eq*BuChE) inhibition, PAMPA-BBB assay and NMDA antagonism.

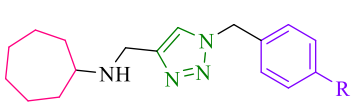

22-28

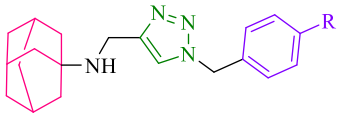

31-37

Comp. No	R	IC_{50} (µM) ± SE[a]		SI[b]	Pe (10^{-6} cm s^{-1})[c]	Permeability prediction (CNS+/-) [d]	NMDA (GluN1-1a/GluN2B) IC_{50} in µM
		*ee*AChE IC_{50} in µM	*eq*BuChE IC_{50} in µM				
22B	H	1.415 ± 0.009	11.354 ± 0.022	8.02	7.20 ± 0.041	CNS+	ND
23B	Br	0.550 ± 0.013	17.296 ± 0.001	31.44	6.72 ± 0.014	CNS+	38.17 ± 0.18
24B	Chloro	0.607 ± 0.014	16.471 ± 0.012	27.13	6.84 ± 0.052	CNS+	ND
25B	Fluoro	1.824 ± 0.003	10.502 ± 0.007	5.75	8.42 ± 0.037	CNS+	97.29 ± 0.16
26B	Methyl	1.219 ± 0.009	19.302 ± 0.015	15.83	7.35 ± 0.017	CNS+	63.65 ± 0.16
27B	Isopropyl	1.518 ± 0.003	15.701 ± 0.021	10.34	7.24 ± 0.047	CNS+	216.55 ± 0.97
28B	Nitro	4.637 ± 0.010	19.210 ± 0.011	4.14	6.31 ± 0.031	CNS+	115.63 ± 0.14
31B	H	0.360 ± 0.013	4.715 ± 0.014	13.09	6.95 ± 0.024	CNS+	ND
32B	Br	0.086 ± 0.007	2.546 ± 0.010	29.60	8.75 ± 0.017	CNS+	9.88 ± 0.15
33B	Chloro	0.135 ± 0.009	3.797 ± 0.013	28.12	8.24 ± 0.034	CNS+	10.92 ± 0.06
34B	Fluoro	0.194 ± 0.017	3.271 ± 0.018	16.86	7.75 ± 0.025	CNS+	ND
35B	Methyl	0.340 ± 0.018	6.042 ± 0.005	17.77	7.48 ± 0.014	CNS+	196.94 ± 0.16
36B	Isopropyl	0.799 ± 0.009	7.826 ± 0.016	9.79	7.63 ± 0.017	CNS+	79.456 ± 0.14
37B	Nitro	1.608 ± 0.008	9.542 ± 0.005	5.93	6.83 ± 0.052	CNS+	21.77 ± 0.21
DNZ	--	0.031 ± 0.013	0.941 ± 0.026	30.35	8.68 ± 0.021	CNS+	--
MMT	--	--	--	--	6.84 ± 0.042	CNS+	0.99 ± 0.2

[a]Results are reported as the mean IC_{50} ± SEM (n = 3). [b]Selectivity ratio for AChE = (IC_{50} of *eq*BuChE)/(IC_{50} of *ee*AChE). DNZ= Donepezil. [c]Data are expressed as the mean ± SEM (n = 3). [d]Compounds with $Pe > 4.324 \times 10^{-6}$ cm s^{-1} could cross the BBB (CNS+). Compounds with $Pe < 1.846 \times 10^{-6}$ cm s^{-1} could not cross the BBB (CNS−), and compounds with 1.846×10^{-6} cm $s^{-1} < Pe < 4.324 \times 10^{-6}$ cm s^{-1} show uncertain BBB permeation (CNS±).

Table 6.3: Propidium iodide displacement assay.

Comp. No	Displacement of Propidium iodide from AChE PAS (% inhibition)[a]	
	At 10 μM	At 50 μM
32B	20.96 ± 2.08	40.93 ± 1.25
33B	19.96 ± 1.25	34.10 ± 1.09
DNZ	20.34 ± 2.44	36.61 ± 2.1

[a]Data are expressed as the standard deviation (SD) of three independent experiments.

6.2.6 NMDARs antagonistic activity of the novel triazole bridged cycloaryl analogs

Apart from the ChEs, the NMDAR was the other primary target, which was pursued with the design of the triazole bridged cycloaryl analogs. In particular, we inferred that the incorporation of cyclic ring to in the structure of the hybrid should confer this additional activity. To assess the NMDAR antagonist activity of the all synthesized analogs we performed two-electrode voltage clamp electrophysiology experiments on *Xenopus laevis* oocytes. Memantine was served as a control substance in the electrophysiological recordings. To determine the selectivity of the synthesized compounds, serial dilutions were prepared in extracellular solution containing the NMDAR agonists glycine (10 μM) and glutamate (100 μM). After activating the receptors by application of the agonists alone, the compound (to be tested) was applied in increasing concentrations in the presence of the NMDAR agonists and the residual current was measured. The results are shown in Figure 6.2 – 6.6. A dose-inhibition curve was then plotted from the generated data and the corresponding IC_{50} value was calculated using the Hill equation. For the prediction of their inhibitory profiles, all compounds were initially tested on the GluN1-1a/GluN2B subunit combination. The compounds containing adamantine as cyclic ring and para bromo/chloro substituted phenyl (**32B** and **33B**) exhibited better NMDAR inhibition. The adamantine ring was found to be accountable for NMDAR antagonist activity as compared to cycloheptane

ring. In case of adamantine cyclic ring, methyl (**35B**; IC_{50} = 196.94 ± 0.16 μM) and isopropyl (**36B**; IC_{50} = 79.45 ± 0.14 μM) substituted phenyl analogs exhibited depletion of activity.

Among these, **32B** and **33B** showed promising results on the investigated GluN1-1a/GluN2B subunit combination with IC_{50} values of 10.9 ± 0.06 μM and 10.8 ± 0.08 μM, respectively. The tested compounds thus have a similar potency to memantine, for which an IC_{50} value of 0.98 μM was determined. In order to evaluate the selectivity of these two compounds, they were additionally tested on the other GluN2 subunits co-expressed with GluN1-1a. This resulted in a better IC_{50} values, which indicated GluN2B selectivity (**32B**, IC_{50} = 3.41 ± 0.05 μM; **33B**, IC_{50} = 3.29 ± 0.03 μM) (Table 6.4).

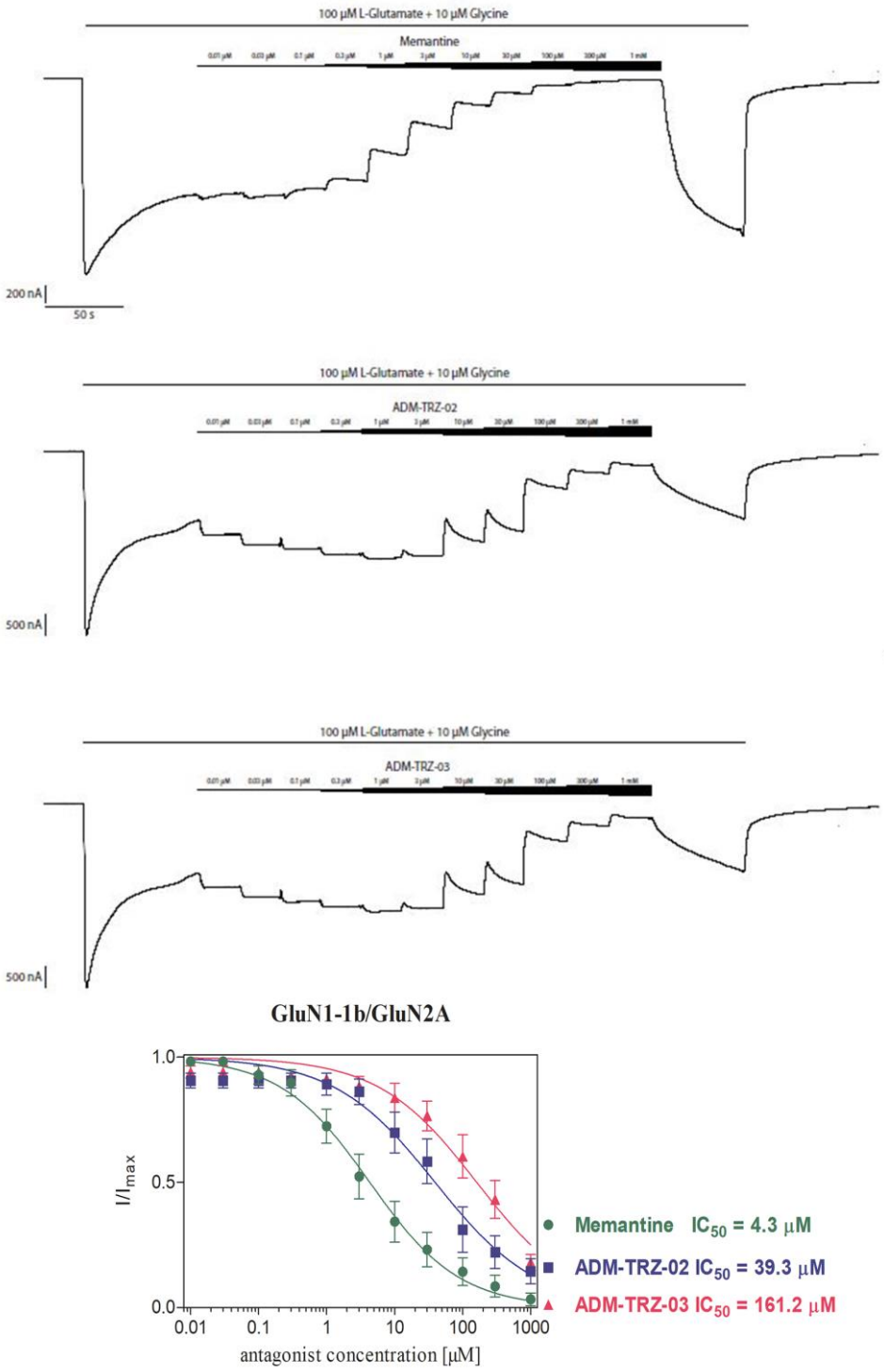

Figure 6.2. Effect of compounds **32B** (ADM-TRZ-02), **33B** (ADM-TRZ-03) and memantine, respectively, on glutamate- and glycine-evoked currents in GluN1-1b/GluN2A-containing receptors. Agonists were diluted in barium Ringer solution and antagonists were tested in agonist solution at shown concentrations (0.01 µM - 1 mM).

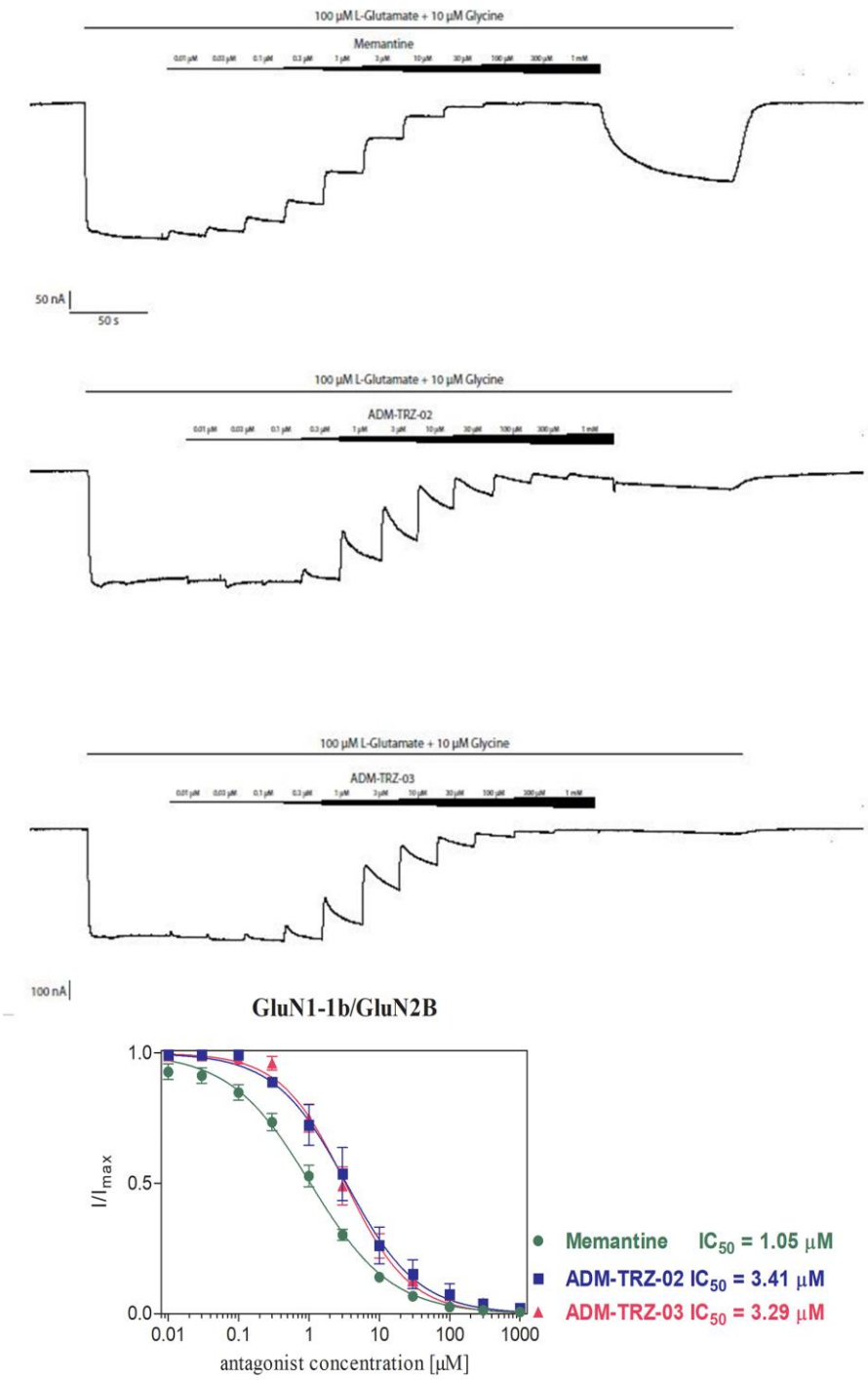

Figure 6.3. Effect of compounds **32B** (ADM-TRZ-02), **33B** (ADM-TRZ-03) and memantine, respectively, on glutamate- and glycine-evoked currents in GluN1-1b/GluN2B-containing receptors. Agonists were diluted in barium Ringer solution and antagonists were tested in agonist solution at shown concentrations (0.01 µM - 1 mM).

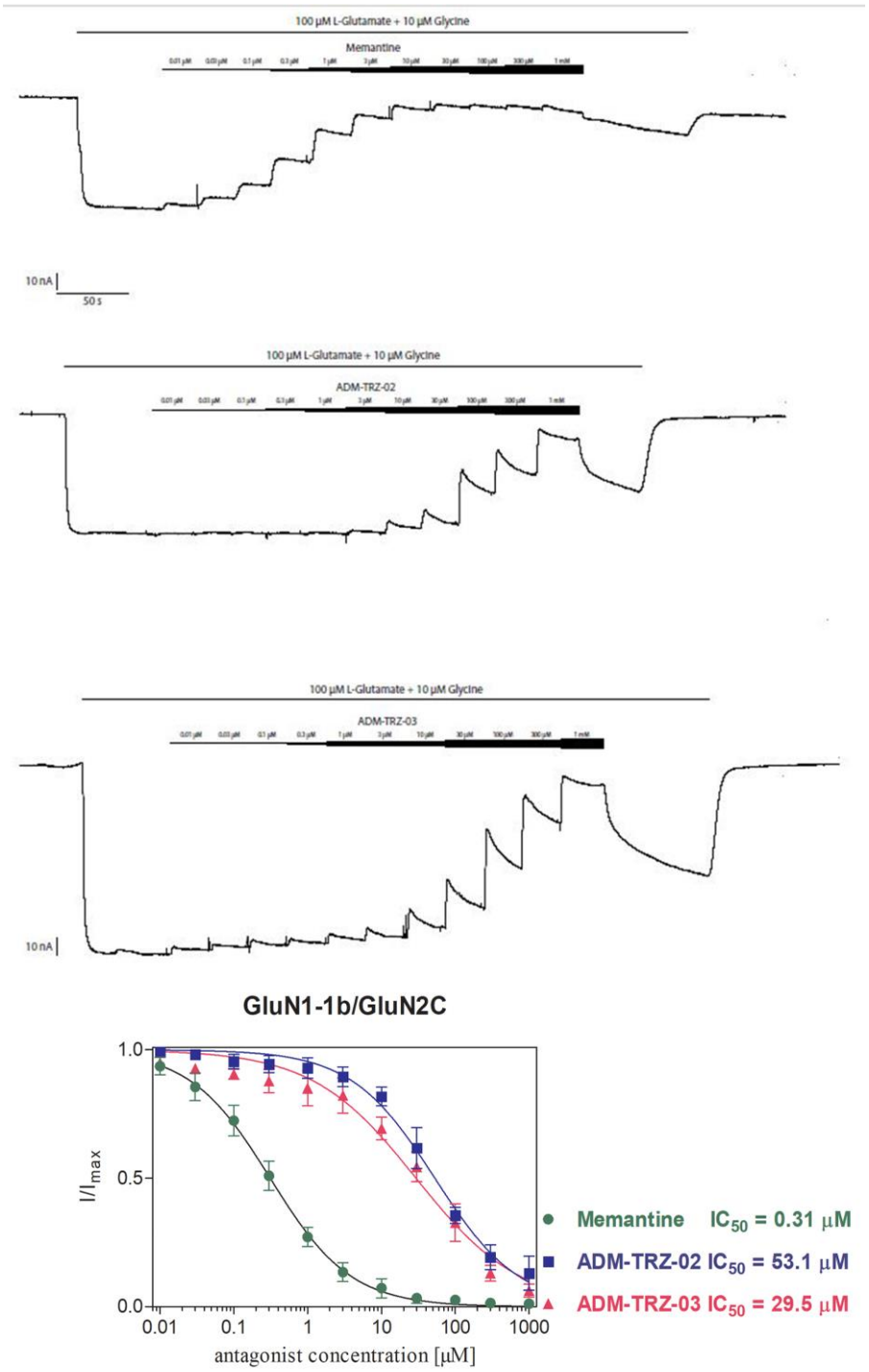

Figure 6.4. Effect of compounds **32B** (ADM-TRZ-02), **33B** (ADM-TRZ-03) and memantine, respectively, on glutamate- and glycine-evoked currents in GluN1-1b/GluN2C-containing receptors. Agonists were diluted in barium Ringer solution and antagonists were tested in agonist solution at shown concentrations (0.01 µM - 1 mM).

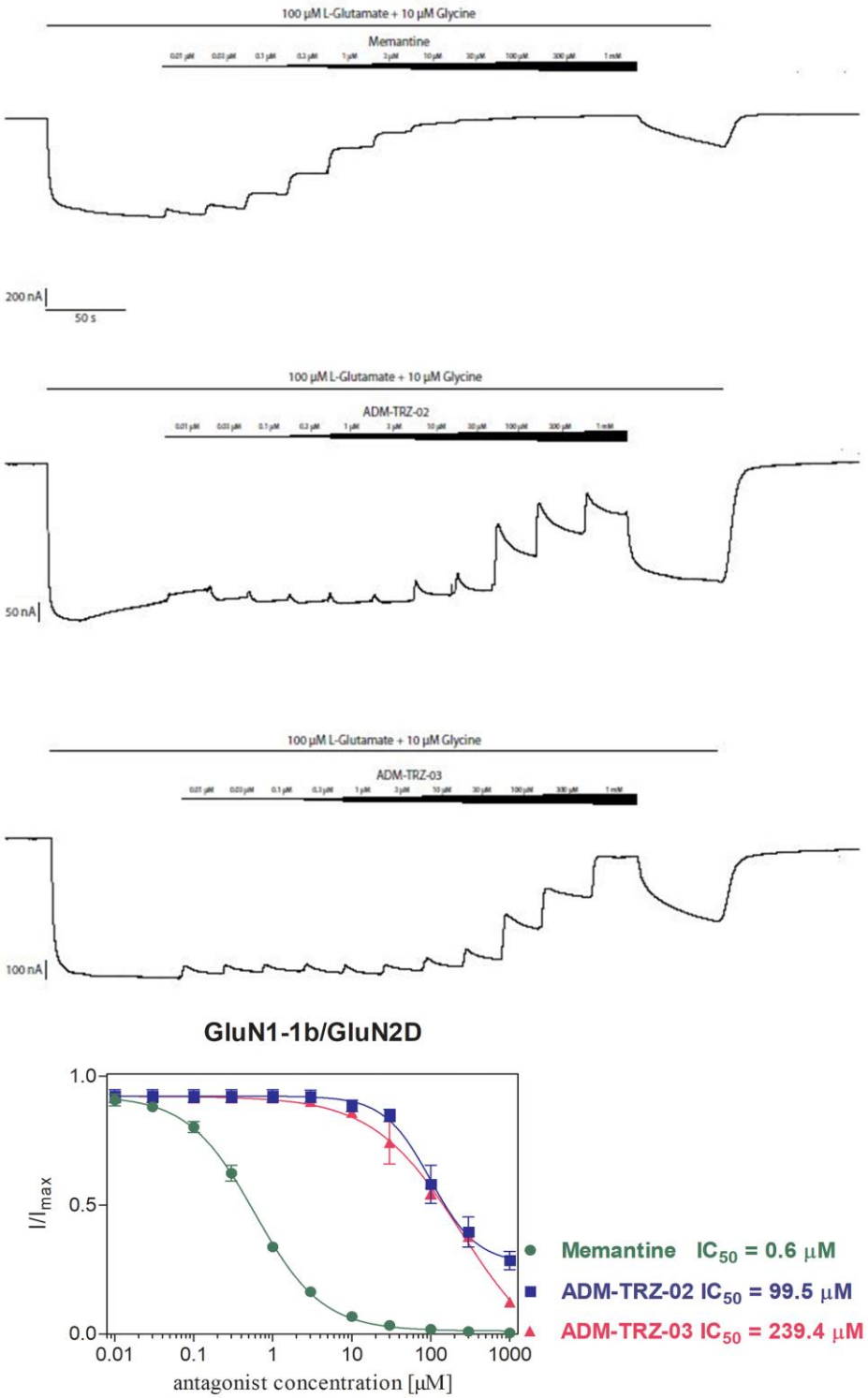

Figure 6.5. Effect of compounds **32B** (ADM-TRZ-02), **33B** (ADM-TRZ-03) and memantine, respectively, on glutamate- and glycine-evoked currents in GluN1-1b/GluN2D-containing receptors. Agonists were diluted in barium Ringer solution and antagonists were tested in agonist solution at shown concentrations (0.01 µM - 1 mM).

Table 6.4. Inhibitory profile of **32B** and **33B** on different NMDAR subunit combinations.

No	NMDA receptor combination	Memantine IC_{50} (μM)	32B IC_{50} (μM)	33B IC_{50} (μM)
1	GluN1-1a/GluN2A	3.6 ± 0.05	52.5 ± 0.05	108.1 ±0.06
2	GluN1-1b/GluN2A	4.3 ± 0.06	39.3 ± 0.08	161.2 ± 0.07
3	GluN1-1a/GluN2B	0.9 ± 0.04	10.9 ± 0.06	10.8 ± 0.08
4	**GluN1-1b/GluN2B**	**1.05 ± 0.03**	**3.41 ± 0.05**	**3.29 ± 0.03**
5	GluN1-1a/GluN2C	0.22 ± 0.12	90.2 ± 0.11	143.0 ± 0.23
6	GluN1-1b/GluN2C	0.31 ± 0.04	53.1 ± 0.05	29.5 ± 0.07
7	GluN1-1a/GluN2D	0.4 ± 0.03	112.4 ± 0.13	788.9 ± 0.24
8	GluN1-1b/GluN2D	0.6 ± 0.02	99.5 ± 0.07	239.4 ± 0.18

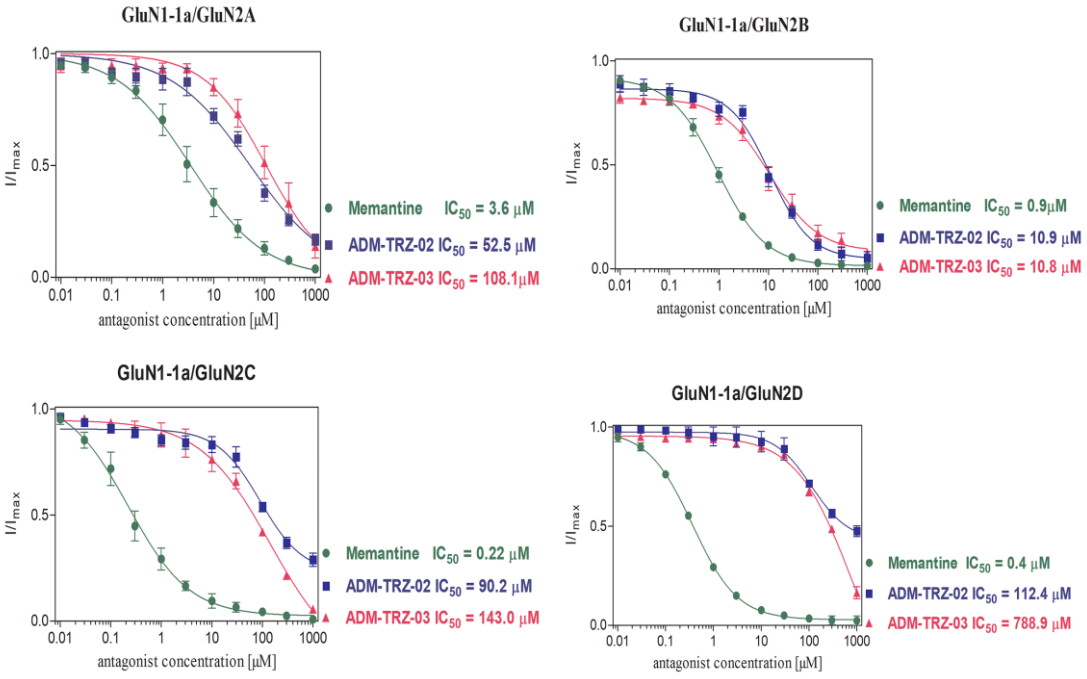

Figure 6.6. Effect of compounds **32B** (ADM-TRZ-02), **33B** (ADM-TRZ-03) and memantine, respectively, on glutamate- and glycine-evoked currents in GluN1-1a/GluN2A-D-containing receptors.

A similar selectivity pattern was also observed while co-expressing the other four GluN2 subunits with the GluN1-1b splice variant, albeit mostly with slightly lower IC_{50} values. The two analogs (**32B** and **33B**) were evaluated for further biological profiling.

6.2.7 Self-induced and AChE induced $A\beta_{1-42}$ aggregation

The deposition and aggregation of Aβ can be considered as a major unfavourable factor in AD. The results of PI displacement assay signified the remarkable binding capability of compounds **32B** and **33B** with PAS-AChE, and it is a known fact that PAS binding of the inhibitor will not only result in AChE inhibition but also have a significant role in prevention of Aβ aggregation [Inestrosa et al. 1996]. The anti-Aβ aggregation activity of these compounds were determined by thioflavin T assay in self- and AChE-induced experiments. The tests were performed at three varied concentration ratios of Aβ and inhibitor (10:5 μM, 10:10 μM, and 10:20 μM, respectively) and the results are reported as normalized fluorescence intensity (NFI) (Figure 6.7. A and B). The results demonstrated the concentration-dependent inhibition of Aβ aggregation with the maximum activity being observed at 20 μM inhibitor concentration (Aβ:inhibitor, 10:20 μM). A slightly higher Aβ inhibition for compound **33B** than DNZ was observed, while compound **32B** displayed remarkable anti-Aβ aggregatory activity in self- and AChE-induced experiments. The observed results were in accordance with the assays of hAChE, hBChE, and PI displacement.

6.2.8 Neuroprotection studies on SH-SY5Y cell lines

To ascertain the neuroprotective profile of compounds **32B** and **33B**, cell viability assay based on MTT was performed on neuroblastoma SHSY5Y cell lines. Aβ peptide (10μM) was used to promote the toxicity on cell lines. The neuroprotection was determined at concentrations of 0.1, 1, 10, and 100 μM of test compounds with parallel

to the standard drug DNZ (0.1 and 1 μM). The outcome of the assay demonstrated a non-significant reduction in cell viabilities toward neuroblastoma cell lines by both compounds (**32B** and **33B**) up to the maximum tested concentration of 10 μM (Figure 6.8). The results ascertained that both compounds (**32B** and **33B**) were neuroprotective in nature and can be considered for further preclinical investigations.

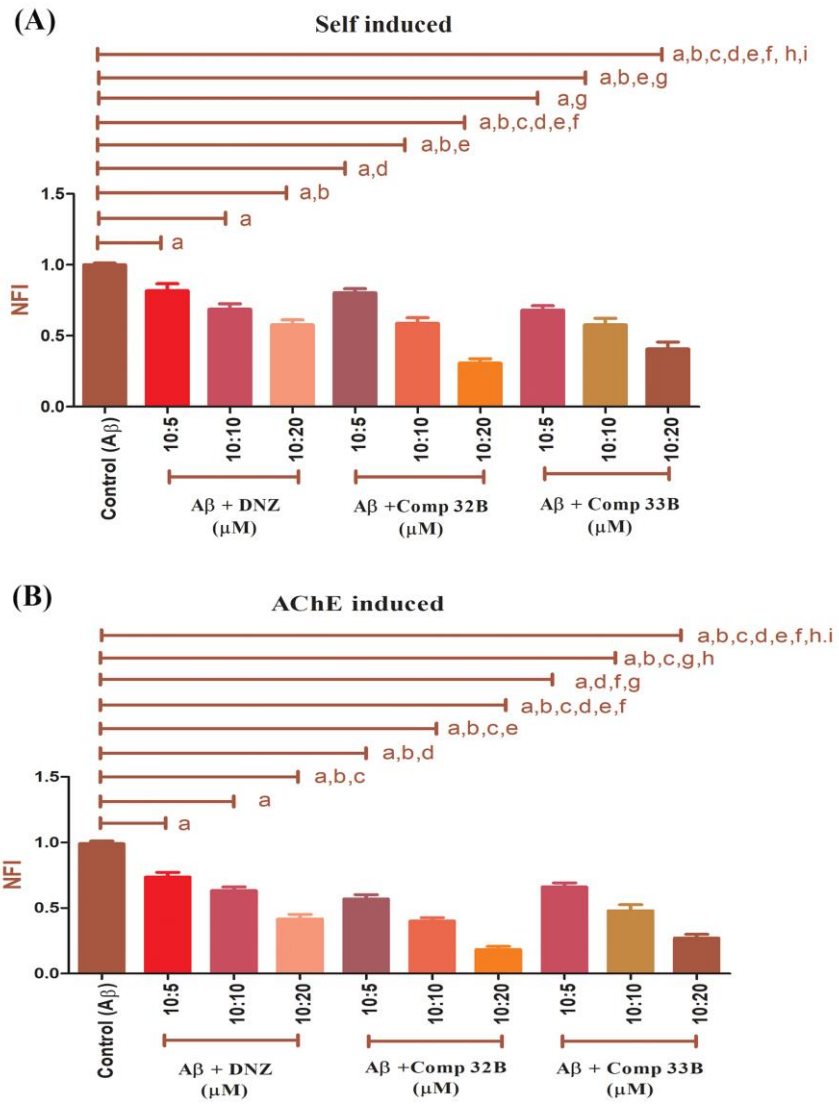

Figure 6.7. Effect of compounds **32B** and **33B** on Aβ aggregation. (A) Self-induced and (B) AChE-induced Aβ aggregation. Bars are showing the normalized fluorescence intensity (NFI) as the mean ± SEM of three separate experiments. [a]$p < 0.05$ compared to control (Aβ), [b]$p < 0.05$ compared to Aβ + DNZ (10:5), [c]$p < 0.05$ compared to Aβ + DNZ (10:10), [d]$p < 0.05$ compared to Aβ + DNZ (10:20), [e]$p < 0.05$ compared to Aβ + comp

32B (10:5), [f]p< 0.05 compared to Aβ + comp **32B** (10:10), [g]p< 0.05 compared to Aβ + comp **32B** (10:20), [h]p< 0.05 compared to Aβ + comp **33B** (10:5), [i]p< 0.05 compared to Aβ + comp **32B** (10:10) (One-way ANOVA followed by Newman - Keuls test).

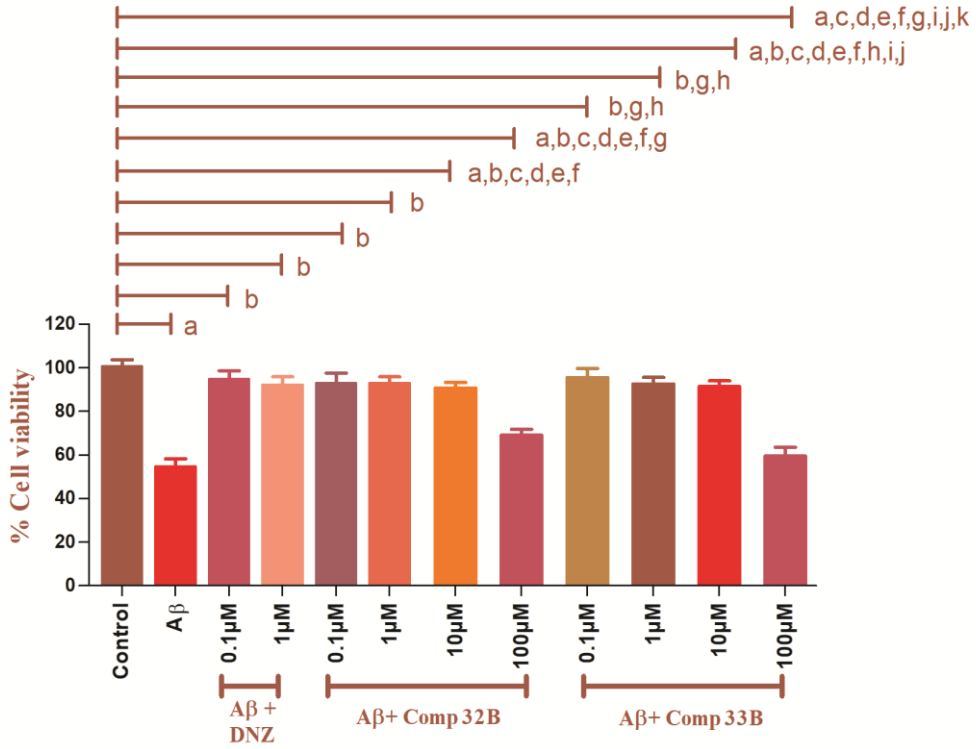

Figure 6.8. Neuroprotection assay on SH-SY5Y cell lines with Compounds **32B** and **33B.** Bars display the mean ± SEM for three different experiments. . [a]p< 0.05 compared to control, [b]p< 0.05 compared to Aβ, [c]p< 0.05 compared to Aβ + DNZ (0.1 μM), [d]p< 0.05 compared to Aβ + DNZ (1 μM), [e]p< 0.05 compared to Aβ + comp **32B** (0.1 μM), [f]p< 0.05 compared to Aβ + comp **32B** (1 μM), [g]p< 0.05 compared to Aβ + comp **32B** (10 μM), [h]p< 0.05 compared to Aβ + comp **32B** (100 μM), [i]p< 0.05 compared to Aβ + comp **33B** (0.1 μM), [j]p< 0.05 compared to Aβ + comp **33B** (1 μM), [k]p< 0.05 compared to Aβ + comp **33B** (10 μM) (One-way ANOVA followed by Newman - Keuls test).

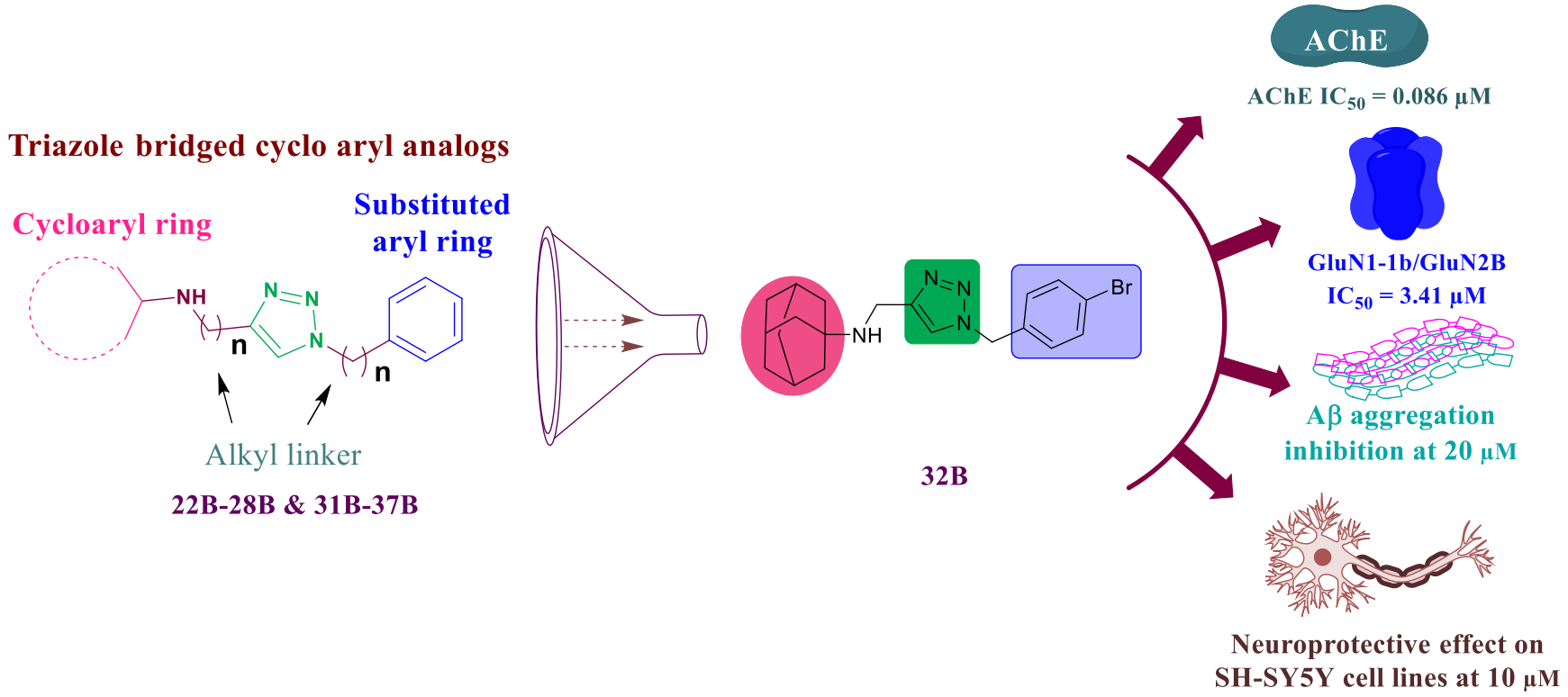

Figure 6.9. Overview of discovery of triazole bridged aryl adamantane analogs.